Materials Chemistry

Cite this: J. Mater. Chem., 2012, 22, 10356

www.rsc.org/materials

PAPER

One-dimensional metal–organic framework photonic crystals used as platforms for vapor sorption†

Florian M. Hinterholzinger,‡[a] Annekathrin Ranft,‡[bc] Johann M. Feckl,[a] Bastian Rühle,[a] Thomas Bein*[a] and Bettina V. Lotsch*[bc]

Received 5th November 2011, Accepted 28th March 2012
DOI: 10.1039/c2jm15685g

We present the fabrication of one-dimensional photonic crystals (Bragg stacks) based on a microporous metal–organic framework material and mesoporous titanium dioxide. The Bragg stack heterostructures were obtained using two complementary synthesis approaches utilizing the bottom-up assembly of heterogeneous, *i.e.* two-component photonic crystal multilayer structures. Zeolitic imidazolate framework ZIF-8 and mesoporous titanium dioxide were chosen as functional components with different refractive indices. While ZIF-8 is intended to impart molecular selectivity, mesoporous TiO_2 is used to ensure high refractive index contrast and to guarantee molecular diffusion within the Bragg stack. The combination of micro- and mesoporosity within one scaffold endows the 1D-MOF PC with characteristic adsorption properties upon exposure to various organic vapors. In this context, the sorption behavior of the photonic material was studied as a function of partial pressure of organic vapors. The results show that the multilayered photonic heterostructures are sensitive and selective towards a series of chemically similar solvent vapors. It is thus anticipated that the concept of multilayer heterogeneous photonic structures will provide a versatile platform for future selective, label-free optical sensors.

Introduction

Metal–organic frameworks represent a class of hybrid materials with promising properties for various applications.[1–5] In particular, the modular tailorability, the rich host–guest interactions, and the widely tunable sorption behavior make MOFs attractive candidates for chemical sensing.[6,7] However, only a few reports are dealing with MOF-based sensors,[8,9] in which the intrinsic framework luminescence[10–14] or the refractive index modulation of Fabry–Pérot interference peaks have been explored for signal transduction.[15] The tunability of the effective refractive index (RI) of MOFs *via* adsorption of guests inspired us to correlate these properties with the underlying optics of photonic crystals (PCs), which are composed of alternating dielectric layers featuring periodic changes in their effective refractive indices.[16–18]

One-dimensional assemblies, which represent the structurally simplest form of photonic crystals, are also known as Bragg stacks (BS) or Bragg mirrors. 1D-PC multilayer structures interacting with visible light require layer thicknesses corresponding to optical wavelengths.[19] As a consequence of the periodicity in the dielectric function, specific wavelengths are efficiently reflected due to diffraction and interference of incident light at each interface of the periodically stacked composite.[20] Enhanced reflectivity is achieved by increasing the number of bilayers or by choosing dielectric materials featuring a high refractive index contrast (Scheme 1).[21]

Currently, intensive research efforts are focused on the development of tunable optical sensors with a label-free operation and compact set-up. There are several approaches ranging from plasmonic noble metal nanotubes[22] or field effect transistors based on reduced graphene[23] to Bragg stacks built up from an alternating polymer architecture,[24] which deal with the implementation of these materials as tunable and label-free sensors. In particular, detection platforms based on Bragg stacks can be realized by translating stimuli-induced optical thickness changes of the constituent materials into a color change of the multilayer photonic structure. So far, several studies are dealing with tailor-made inorganic or hybrid materials to implement functionality within one-dimensional photonic crystals.[25] While there are several examples of versatile SiO_2–TiO_2 systems,[26–28]

[a]*Department of Chemistry and Center for NanoScience (CeNS), University of Munich (LMU), Butenandtstraße 11 (E), 81377 München, Germany. E-mail: bein@lmu.de; Web: http://www.cup.uni-muenchen.de/pc/bein; Fax: +49 89-2180-77622*
[b]*Max Planck Institute for Solid State Research, Heisenbergstraße 1, 70569 Stuttgart, Germany. E-mail: b.lotsch@fkf.mpg.de; Fax: +49 711-689-1612*
[c]*Department of Chemistry and Center for NanoScience (CeNS), University of Munich (LMU), Butenandtstraße 5-13 (D), 81377 München, Germany*

† Electronic supplementary information (ESI) available: X-ray diffraction, TGA/DSC, IR, SEM, TEM and sorption data of bulk ZIF-8 and TiO_2 material as well as SEM, RAIR and ellipsometric data of the Bragg stacks and the reference experiments. See DOI: 10.1039/c2jm15685g

‡ Both authors contributed equally to this work.

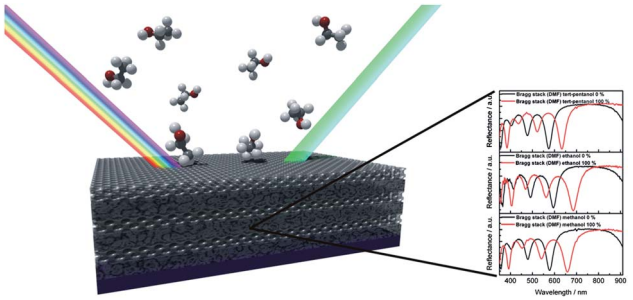

Scheme 1 Schematic representation of a multilayered photonic crystal architecture illustrating the structure- and angle-dependent reflection of incident light as well as the optical response upon exposure to external stimuli.

including both dense and porous morphologies as well as nanoparticle-based Bragg stacks,[29,30] smart hybrid photonic materials with intrinsic functionality are still rare.

In principle, a Bragg stack offers a versatile platform for the detection of molecular interactions and the development of chemical sensors, whereas the realization of chemical selectivity in sensors remains a great challenge.

Very recently, several groups reported a new transduction scheme based on the fabrication of MOF-containing ordered 3D photonic structures.[31,32] The selectivity issue is addressed by integrating metal–organic frameworks into three-dimensional inverse opal structures. While Wu *et al.*[32] employed a colloidal crystal templating approach using a polystyrene opaline "mold", the group of J. Hupp[31] deposited MOF crystals onto a silica template to obtain hybrid MOF–silica colloidal crystal (MOF–SCC) films. The authors have shown that the introduction of an ordered porous structure imparts useful optical features to HKUST-1 and ZIF-8. For MOF–SCC an optical signal displayed by distinct stop band shifts upon analyte sorption is readily observed.

Contrary to 3D photonic materials, we introduce herein a one-dimensional photonic architecture based on a microporous metal–organic framework and titanium dioxide. Thus, an optical transducer system is built, which is used to efficiently convert molecular adsorption into an optical response. As a microporous material, the intensively studied zeolitic imidazolate framework ZIF-8[33] was chosen; this is expected to impart size- and chemo-selectivity and, thus, functionality to the 1D-MOF PC. Complementary material properties in one single platform, such as hydrophobicity/hydrophilicity, dual pore-size regimes, and high refractive index contrast, can be additionally integrated by our combined assembly approach.

Ultimately, the presented results are expected to extend the toolbox for designing nanoporous and at the same time highly selective photonic crystals, to promote our understanding of molecular interactions in porous materials, and to provide novel concepts for label-free chemo-optical sensors.

Experimental

All chemicals (zinc nitrate hexahydrate, 2-methylimidazole; nitric acid (0.1 M), titanium(IV) ethoxide, titanium tetrachloride) as well as solvents are commercially available and were used as received. *Tert*-butyl alcohol was dried over a 4 Å molecular sieve at 28 °C and filtered prior to use.

Route A

Preparation of dense ZIF-8 films. ZIF-8 thin films were prepared on silicon wafers, similar to the approach reported in ref. 14 and 15. The substrates were pre-cleaned in Piranha solution (H_2SO_4/H_2O_2, 70 : 30 (v/v)) at 70 °C for 30 minutes, rinsed with distilled water and dried under nitrogen flow.

For ZIF-8 thin film preparation, 500 mL methanolic stock solutions of $Zn(NO_3)_2 \cdot 6H_2O$ (25 mM, 99%, Aldrich) as well as of 2-methylimidazole (mIm) (50 mM, 99%, Aldrich) were prepared. A ZIF-8 thin film was obtained by immersing the cleaned substrates in a fresh mixture of 10 mL $Zn(NO_3)_2$ stock solution and 10 mL mIm stock solution for 30 minutes at room temperature. For optimization of homogeneity and to enhance surface smoothness, two different strategies were employed. The beakers were either put in an ultrasonic bath or fixed on a shaker during film growth. The as-prepared ZIF-8 thin film was washed with methanol and dried under nitrogen flow. Thicker films could be obtained by simply repeating the process with fresh solutions.

Synthesis of ultrasmall titanium dioxide nanoparticles and film preparation. Titanium dioxide nanoparticles were synthesized as described earlier.[34] In brief, a nonaqueous sol–gel route in *tert*-butyl alcohol under microwave irradiation was used to yield ultrasmall (3 nm), crystalline (anatase), non-agglomerated and highly dispersible nanoparticles.

For all syntheses, titanium tetrachloride (0.7 mL, 6.4 mmol, 99.995%, Aldrich) was dissolved in toluene (5 mL) and added to *tert*-butyl alcohol (15 mL, 160 mmol, Aldrich) under continuous stirring. Microwave heating was performed in microwave autoclaves with an initial heating power of 1200 W (Synthos 3000, Anton Paar). The solution was heated to 80 °C within 1 min and then kept at 50 °C for 20 min resulting in a slightly yellow, transparent solution of nanoparticles. To obtain the fully crystalline nanoparticles, this heating procedure was repeated one more time after a cooling period to room temperature. The solution was then colorless and titanium dioxide could be flocculated by the addition of *n*-heptane (*n*-heptane : *tert*-butanol/toluene 2 : 1 volume ratio; Sigma) and separated by centrifugation at 50 000 rcf for 15 min.

For the preparation of the mesoporous (mp) titania films the nanoparticle pellet (0.4 g) was redispersed in ethanol (8.3 mL) and Pluronic F127 (0.1 g, *BASF*) was added as structure directing agent (SDA).

Fabrication of Bragg stack 1 (BS-1). For the fabrication of Bragg stack 1 (**BS-1**), thoroughly washed and dense ZIF-8 thin films were coated with a fresh colloidal suspension of redispersed ultrasmall titanium dioxide nanoparticles. The films were deposited by spin-coating using a Laurell WS-400B-6NPP-Lite-AS spin-coater at a speed of 5000 rpm to give a film thickness of ~50 nm. To remove the SDA, the films were first heated to 100 °C (3 h ramp, 1 h dwell time) to increase the film stability followed by an extraction of the SDA with ethanol under reflux for 1 h. The complete removal was confirmed by reflection absorption infrared (RAIR) spectroscopy in addition to scanning electron microscopy (SEM) (see ESI, Fig. S11 and S12†).

The whole procedure was repeated 3 times to obtain multiple alternating ZIF-8–mp-TiO_2 architectures.

Route B

Synthesis of ZIF-8 nanoparticles. ZIF-8 nanoparticles were prepared by a modified literature synthesis.[35] In a typical experiment, $Zn(NO_3)_2 \cdot 6H_2O$ (1.03 g, 3.45 mmol, 99%, Grüssing) was dissolved in methanol (70 mL, puriss, Sigma) and rapidly added to a pre-cooled (0 °C) solution of 2-methylimidazole (2.27 g, 27.7 mmol, 99%, Aldrich) in methanol (70.0 mL). The mixture was stirred and cooled constantly throughout the reaction until the solution slowly turned turbid. After 30 min, the nanocrystals were separated from the solvent by centrifugation. Colloidal suspensions of ZIF-8 were obtained by redispersing the particles after centrifugation in DMF (or methanol) (670 mg ZIF-8/1 mL DMF).

Synthesis of titania nanoparticles. Titania nanoparticles were synthesized according to the literature.[36] In a typical procedure, $Ti(OEt)_4$ (6.25 mL, Aldrich) was slowly added to HNO_3 (0.1 M, 37.5 mL, puriss, Acros) under stirring and heated to 80 °C for 8 h. After cooling to room temperature, the opalescent mixture was sonicated for at least 3 h in order to break up agglomerates. Colloidal suspensions of titania in a solvent sufficiently volatile for spin-coating were obtained by repeated collection of the particles by centrifugation and redispersion in DMF (or methanol) (130 mg TiO_2/1 mL DMF).

Fabrication of Bragg stack 2 (BS-2). Silicon wafers were used as substrates for the film deposition by spin-coating. The substrates were pre-cleaned with soap and water and subsequently treated with Piranha solution (H_2SO_4/H_2O_2, 2 : 1). After thoroughly rinsing with deionized water, the wafers were dried under nitrogen flow and stored in ethanol. Before film deposition, the substrates were plasma-cleaned and rinsed with ethanol under spinning for 5 s. The preparation of the Bragg reflector was performed by alternatingly spin-coating colloidal suspensions of ZIF-8 and titania onto the substrate at a speed of 4000 rpm (1500 acceleration) for 60 s, starting with ZIF-8. The film thickness was adjusted by the particle concentration in the suspensions and by multiple coating steps. After each deposition, the film was annealed at 200 °C for 30 min.

Characterization

X-ray diffraction (XRD) measurements of powders and thin films were performed using a Bruker D8 (Cu-Kα1 = 1.5406 Å; Cu-Kα2 = 1.5444 Å) in *theta–theta* geometry. The films were measured between 5° and 20° *two theta*, with a step-size of 0.05° *two theta* and a scan-speed of 3° min^{-1}. The data of the powder samples were collected between 5° and 45° *two theta* with a step-size of 0.05° *two theta* and a scan-speed of 0.3° min^{-1}.

SEM micrographs of **BS-1** were recorded with a JEOL JSM-6500F scanning electron microscope (SEM) equipped with an Oxford EDX analysis system; those of **BS-2** with a Merlin (Zeiss) FE-SEM. Ellipsometry measurements were performed with a Woollam M2000D at an angle of 75° in the spectral range of 190–1000 nm. The data were fitted between 350 and 1000 nm using a Cauchy-type material as the model layer. Reflectance measurements were recorded with the same ellipsometer using *s*-polarized light at an incident angle of 75°.

The recording of isotherms was performed at ambient temperature using a home-made Labview-controlled gas mixer. Digital mass flow controllers (W-101A-110-P, F-201C, Bronkhorst High-Tech) ensured the accurate dosing of the carrier gas nitrogen and the liquid analyte, which was vaporized in a controlled evaporation and mixing element (W-101A, Bronkhorst High-Tech). Partial pressures (p) were calculated using the van der Waals equation.[28,37] The relative pressure pp_0^{-1} relates to the saturation pressure p_0.

Results and discussion

Bragg stack preparation and structural properties

Two different strategies were employed for the fabrication of 1D-MOF photonic crystals consisting of either dense or porous ZIF-8 layers, and differently sized mesoporous titanium dioxide nanoparticle derived films. Stability, pore accessibility as well as high optical quality multilayer films are key requirements for the fabrication of analyte-responsive transducer systems. Those features were addressed by the choice of suitable deposition and post-treatment parameters. For the mp-TiO_2 deposition in **BS-1**, both a complete removal of the template (see ESI, Fig. S11 and S12†) as well as minimum etching of the ZIF-8 underlayer had to be achieved. In Fig. 1 the X-ray diffraction patterns of both 3-bilayer Bragg stacks (photographs shown in Fig. 2) are depicted and compared to simulated data. The mild annealing temperatures employed in either case, in addition to the solvent extraction carried out under non-acidic conditions (**BS-1**), retain the crystallinity and stability of the ZIF-8 layers. The diffraction patterns of the multilayered ZIF-8–TiO_2 composites show excellent agreement with the simulated ZIF-8 data, apart from peak broadening, indicating a slightly smaller grain size of the ZIF-8 crystals within the BSs.

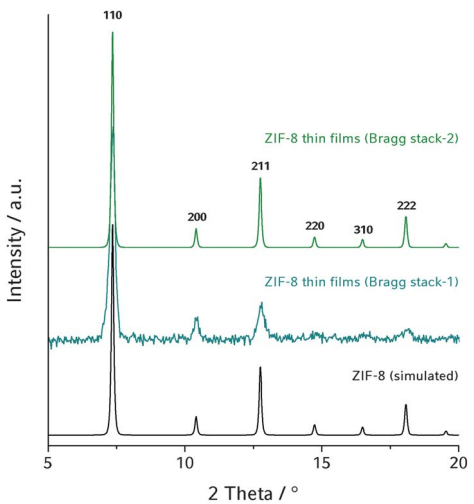

Fig. 1 X-ray diffraction patterns (background corrected) of the 3-bilayer Bragg stack 1 (middle) as well as of Bragg stack 2 (top) after temperature treatment and complete removal of the structure-directing agent (F127), compared to simulated data (bottom line).

In contrast to **BS-1**, which features dense ZIF-8 layers, **BS-2** is composed of ZIF-8 nanocrystals (approx. 50 nm diameter, see ESI, Fig. S2†), forming uniform layers, and nanoparticle-based TiO_2 layers with TiO_2 particles around 10–15 nm in diameter. Therefore, we expect **BS-2** to exhibit a fairly high degree of textural mesoporosity in both layers, in addition to the intrinsic microporosity provided by the ZIF-8 crystals.

The coexistence of both materials embedded in the 1D-MOF PC structure is confirmed by scanning electron microscopy (SEM). In Fig. 3 representative 3-bilayer Bragg stacks composed of alternating microporous ZIF-8 layers and porous titania layers deposited on a silicon substrate are depicted. The differently prepared Bragg stacks exhibit a ZIF-8 layer thickness of approximately 70 nm in **BS-1** and about 200 nm in **BS-2**, respectively. TiO_2 layers deposited on each ZIF-8 film have a thickness of about 50 nm in both Bragg stacks. The cross-sectional SEM micrographs reveal that both fabrication methods yield fairly uniform layer thicknesses throughout the entire architecture. Fig. 3 also demonstrates the alteration of both materials seen by the differences in material contrast. While the dark layers represent the ZIF-8 material exhibiting a lower electron density, the brighter thin films consist of TiO_2 nanoparticles. Not only the deposition of ZIF-8 layers on silicon, as already shown by several groups,[15,38] but also adhesion between ZIF-8 and mesoporous/nanoparticle titania layers was achieved using our dual assembly approach. In contrast to the deposition of MOF material on inverse opal structures,[31,32] no surface modification is necessary when preparing ZIF-8-based one-dimensional photonic structures. Regarding the stability and crystallinity of the multilayered Bragg stacks, no delamination or amorphization upon heating, extraction or adsorption of volatile species is observed, which is consistent with the corresponding XRD results (see Fig. 1). In conclusion, robust, uniform and high-optical quality multilayered photonic crystals composed of two different materials with varying morphologies can reproducibly be fabricated and thus provide the basis for chemical sensing studies.

Vapor adsorption and optical sensing

The combination of a microporous MOF material with mesoporous metal oxide layers is supposed to endow the material with a unique combination of size-selectivity and analyte sensitivity. The integration of both morphologies within one photonic structure is expected to act as a molecular sieving platform, readily adsorbing analyte molecules with small kinetic diameters in both layers, whereas the access of larger guests is exclusively possible into the mesoporous titania layers. Essentials such as high specific surface areas, pore accessibility, efficient diffusion and molecular sieving abilities are all addressed by our highly porous 1D-MOF photonic crystals.

Fig. 2 Photographs of 3-bilayer Bragg stack 1 (left) and Bragg stack 2 (right) on a 5 × 2.5 cm^2 Si substrate in air.

The optical response of the 1D-MOF PCs to guest adsorption was investigated by performing sorption experiments of volatile analyte molecules. According to the optical Bragg equation, sorption of volatile species into the porous layers influences the effective refractive index of a bilayer by which analyte-induced color changes can be efficiently monitored. In Fig. 4 the reflectance spectra of both Bragg stacks are demonstrated. Here, the optical response is triggered by the adsorption of ethanol vapor at the highest partial pressure ($p/p_0 \approx 1.0$), which entails pronounced red-shifts of the Fabry–Pérot fringe of **BS-1** from $\lambda \approx 585$ to $\lambda \approx 630$ nm as well as of the stop band of **BS-2**, derived from nanoparticles redispersed in DMF, from $\lambda \approx 740$ to $\lambda \approx 840$ nm, respectively. We attribute the significantly larger optical shift of **BS-2** to the thicker ZIF-8 layers and amplified external surface area (and hence accessibility), which underlines the enhanced contribution of the "active" component to the observed overall optical shift of the BS.[39] Compared to the 3D-MOF (HKUST-1) hybrid photonic crystals recently reported by the groups of J. Hupp and G. Li,[31,32] which show optical shifts of 9 nm and 16 nm upon ethanol sorption, respectively, a significant increase with respect to the optical response can be monitored in our system. However, when infiltrating 30 μm thick polystyrene template films with ZIF-8, Wu *et al.* observed a distinct shift of about 75 nm upon methanol adsorption.[32] Compared to the inherently smaller absolute shifts observed with **BS-1**, which are presumed to result from the significantly smaller thickness of the ZIF-8 films, an even higher sensitivity upon sorption of organic vapors can be deduced from the reflectance spectrum of **BS-2** (Fig. 4 and S21†). Note that only a short heating period of 15 minutes at 200 °C was applied to Bragg stack 2 prior to the sorption experiments compared to the activation procedure reported by Wu *et al.*[32] The samples were additionally subjected to a high-rate flow of dry nitrogen (Varian Chrompack Gas-clean Moisture Filter CP 17971, outlet concentration <0.1 ppm), which highlights the facile analyte uptake and release during a series of sorption measurements.

Analyte-induced variations of the optical thickness give rise to distinct optical shifts not only for ethanol and methanol but also for other larger analytes such as isobutanol and *tert*-pentanol. Adsorption isotherms monitoring the optical shift as a function of relative vapor pressure were recorded for **BS-2** (Fig. 5c) as well as for the dense and porous ZIF-8 films as reference (Fig. 5a and b). The latter show that the smaller alcohols are readily adsorbed by this MOF, including analyte molecules with larger kinetic diameters compared to the aperture size of ZIF-8 (3.4 Å).[33] These results are consistent with literature data, as it was previously shown that molecules such as ethanol or isobutanol exhibiting kinetic diameters of 4.5 Å (ref. 40) and 5 Å (ref. 41) are readily adsorbed owing to the flexibility of the pore apertures in ZIF-8.[41,42] Hence, *tert*-pentanol (2-methyl-1-propanol) was chosen as a sterically demanding analyte molecule with a kinetic diameter larger than 5 Å.[43] The dense ZIF-8 reference film only shows a minute optical shift of 4 nm, which is consistent with the almost complete exclusion of *tert*-pentanol from the ZIF-8 pore system (Fig. 5a). The nanoparticle-based ZIF-8 film shows a larger

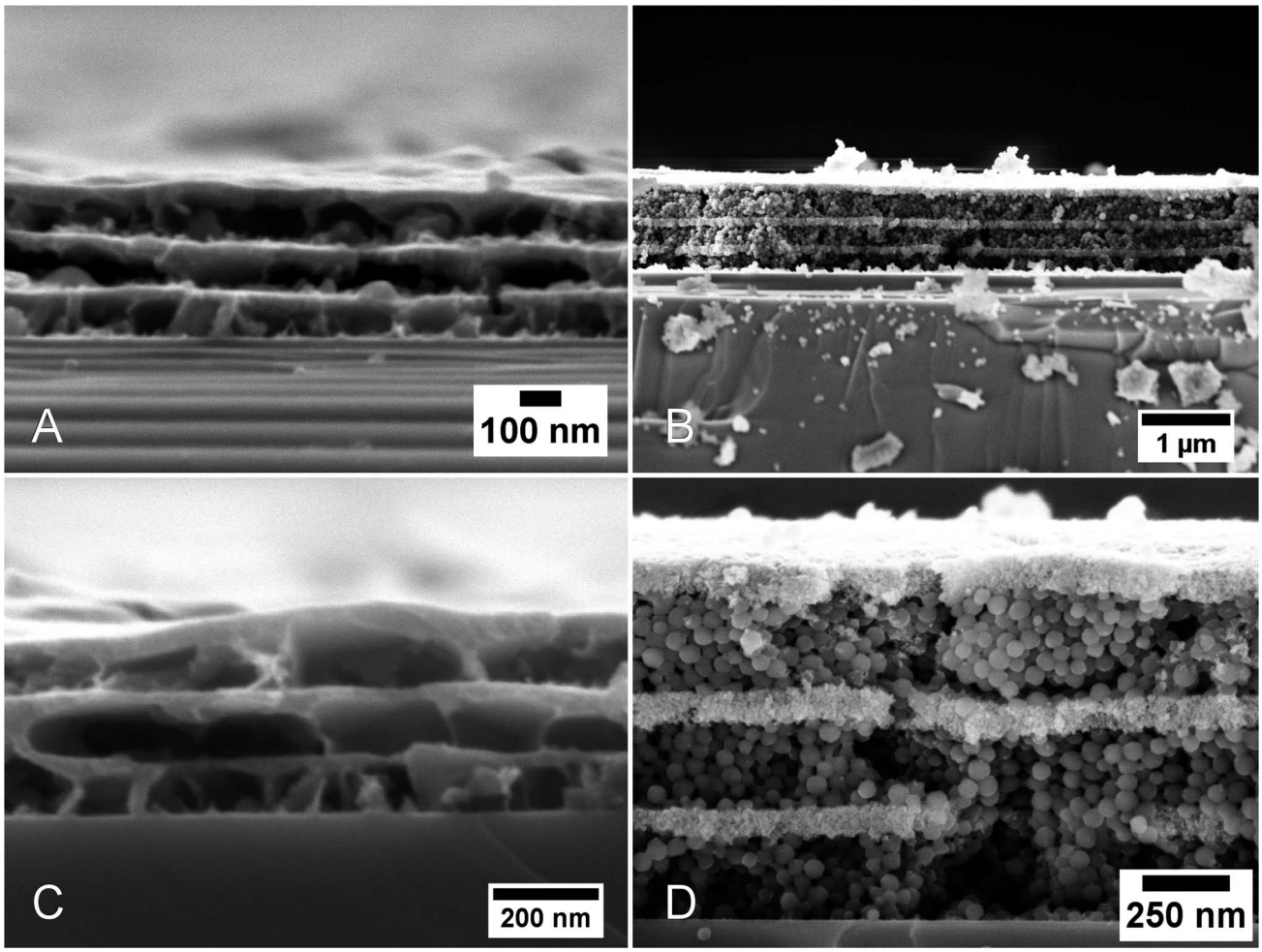

Fig. 3 Scanning electron micrographs showing cross-sections of both 3-bilayer Bragg stacks with an average film thickness of ~50 nm for each titania layer and ~70 nm for each ZIF-8 layer for **BS-1** (A and C) as well as for **BS-2** (DMF, B and D) exhibiting a layer thickness of ~50 nm for each titania layer and ~200 nm for ZIF-8 layers, respectively. ZIF-8–TiO_2-BSs are depicted for different magnifications (A: ×80 000; B: ×15 000; C: ×100 000; D: ×60 000).

optical shift of about 30 nm at the highest partial pressure ($p/p_0 \approx 1.0$, Fig. 5b), which is in agreement with the presence of a significant degree of textural mesoporosity.

In order to probe the host–guest interactions within the comparatively more complex Bragg stack environment, optical adsorption isotherms were recorded exemplarily for **BS-2**, as

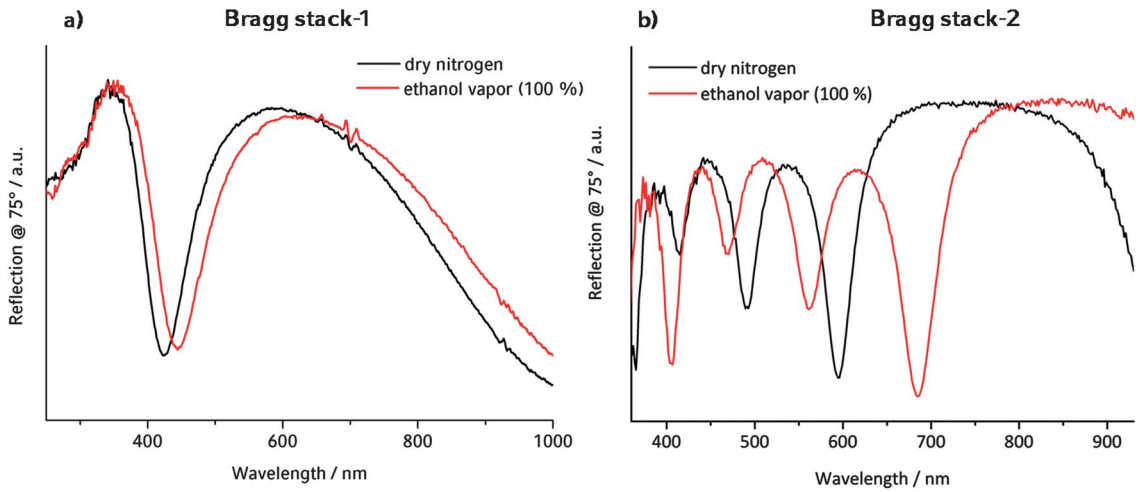

Fig. 4 Reflectance spectra of Bragg stack 1 (a) and Bragg stack 2 (DMF) (b) illustrating the optical shift upon ethanol exposure recorded at the highest partial pressure ($p/p_0 \approx 1.0$).

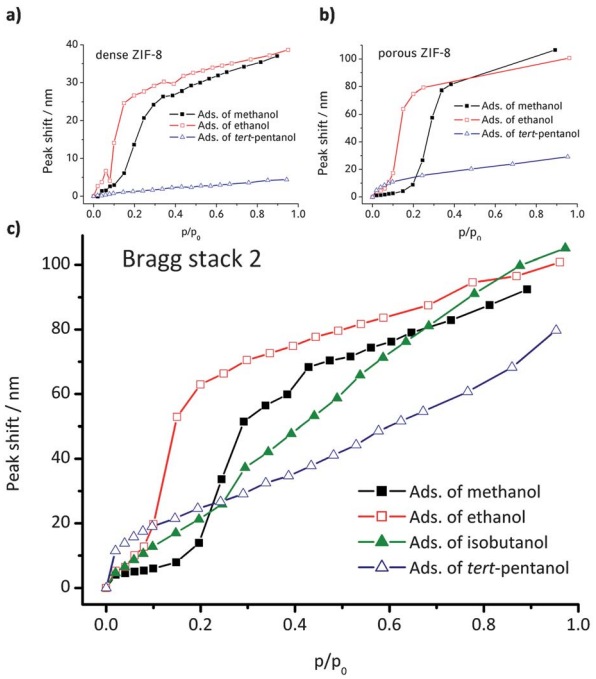

Fig. 5 Optical vapor sorption isotherms demonstrating the adsorption performance of (a) dense and (b) nanoparticulate ZIF-8 reference samples as well as of (c) **BS-2** (DMF) during exposure to a series of alcohol vapors.

depicted in Fig. 5c. Specifically, the initial stages during adsorption of alcohol vapors and the expected pore size-specific adsorption isotherms achieved through the incorporation of different porosities are of key interest.

During the first two dosing steps the 1D-MOF Bragg stack rapidly responds to all analyte molecules, indicated by varying red-shifts ranging from 5 to 15 nm (Fig. 5c). At a partial pressure of $p/p_0 = 0.1$ and $p/p_0 = 0.2$, respectively, a steep increase in the methanol and ethanol isotherms is observed. However, a larger optical shift is recorded for ethanol, which is attributed to more beneficial interactions between ethanol and ZIF-8 owing to the larger hydrophobicity of ethanol compared to that of methanol. At the respective threshold pressures, pronounced optical shifts of about 50–60 nm are recorded, which gradually increase up to saturation pressure. The S-shaped isotherms upon methanol and ethanol adsorption recorded for both the single ZIF-8 films and for **BS-2** are in good agreement with the results obtained by Remi *et al.*[44] The authors attribute the S-shaped isotherms to changes in the framework triggered by interactions with guest-molecules, which was additionally confirmed and described elsewhere.[42] In contrast to the distinct S-shaped isotherms, isobutanol sorption experiments yield an almost linearly increasing adsorption behavior with an absolute shift of about 100 nm at the highest partial pressure. In contrast, the adsorption isotherm of *tert*-pentanol exhibits a convex shape featuring the highest uptake during the first dosing steps, which we attribute to the textural porosity of both ZIF-8 and titania layers arising from the nanoparticle architecture, as seen also for the porous ZIF-8 film (Fig. 5b). However, this analyte exhibits the smallest *overall* uptake, which is consistent with the exclusion of *tert*-pentanol from the ZIF-8 pores, as demonstrated also for the individual ZIF-8 films. In contrast, the smaller analytes (methanol, ethanol, isobutanol) are more readily adsorbed owing to their smaller kinetic diameters.

As discussed above, an important finding is the fact that distinctly shaped isotherms are obtained for each of the four analytes over the entire relative pressure range, as additionally demonstrated by reproduced sorption experiments using Bragg stacks derived from two different synthesis batches (see ESI, Fig. S22†). The characteristic sorption behavior indicates a high degree of chemical selectivity inherent to the MOF-BS, which is especially noticeable at low relative pressures. Comparison of the shapes of the isotherms for the BS and the individual ZIF-8 thin films (Fig. 5) confirms that the optical response is dominated by ZIF-8.

Conclusions

In summary, a one-dimensional MOF-based photonic crystal heterostructure with embedded micro- and mesoporosity is presented. The fabrication of the 1D-MOF PC was achieved *via* two different inexpensive bottom-up synthesis approaches. The strategy of combining a microporous MOF material with mesoporous titanium dioxide layers provides the basis for a highly sensitive signal transduction scheme with an amplified overall optical response, while maintaining high chemical specificity. Hence, molecular recognition is translated into a readable optical signal without the use of any reporter systems.

The concept of MOF-based one-dimensional photonic crystal structures extends the scope of chemoselective optical signal transducer systems. We anticipate a generalization of the assembly of 1D photonic materials in terms of the large variety and tunability of MOFs or related materials. Thus, we believe that the above proof-of-concept experiments provide a basis for the design of highly sensitive and chemically selective optical sensors.

Acknowledgements

Financial assistance from DFG (SPP 1362), the Center for Nanoscience (CeNS) and the cluster of excellence Nanosystems Initiative Munich (NIM) is gratefully acknowledged. The authors thank Dr Steffen Schmidt and Viola Duppel for assistance with SEM data acquisition.

Notes and references

1 O. M. Yaghi, M. O'Keeffe, N. W. Ockwig, H. K. Chae, M. Eddaoudi and J. Kim, *Nature*, 2003, **423**, 705–714.
2 G. Ferey, *Chem. Soc. Rev.*, 2008, **37**, 191–214.
3 U. Mueller, M. Schubert, F. Teich, H. Puetter, K. Schierle-Arndt and J. Pastre, *J. Mater. Chem.*, 2006, **16**, 626–636.
4 J.-R. Li, R. J. Kuppler and H.-C. Zhou, *Chem. Soc. Rev.*, 2009, **38**, 1477–1504.
5 S. T. Meek, J. A. Greathouse and M. D. Allendorf, *Adv. Mater.*, 2011, **23**, 249–267.
6 C. Scherb, J. J. Williams, F. Hinterholzinger, S. Bauer, N. Stock and T. Bein, *J. Mater. Chem.*, 2011, **21**, 14849–14856.
7 O. Shekhah, J. Liu, R. A. Fischer and C. Woll, *Chem. Soc. Rev.*, 2011, **40**, 1081–1106.
8 M. D. Allendorf, C. A. Bauer, R. K. Bhakta and R. J. T. Houk, *Chem. Soc. Rev.*, 2009, **38**, 1330–1352.
9 L. E. Kreno, K. Leong, O. K. Farha, M. Allendorf, R. P. Van Duyne and J. T. Hupp, *Chem. Rev.*, 2011, **112**, 1105–1125.

10 H. Xu, F. Liu, Y. Cui, B. Chen and G. Qian, *Chem. Commun.*, 2011, **47**, 3153–3155.
11 B. Chen, L. Wang, Y. Xiao, F. R. Fronczek, M. Xue, Y. Cui and G. Qian, *Angew. Chem.*, 2009, **121**, 508–511.
12 B. Gole, A. K. Bar and P. S. Mukherjee, *Chem. Commun.*, 2011, **47**, 12137–12139.
13 K. C. Stylianou, R. Heck, S. Y. Chong, J. Bacsa, J. T. A. Jones, Y. Z. Khimyak, D. Bradshaw and M. J. Rosseinsky, *J. Am. Chem. Soc.*, 2010, **132**, 4119–4130.
14 Y. Takashima, V. M. Martínez, S. Furukawa, M. Kondo, S. Shimomura, H. Uehara, M. Nakahama, K. Sugimoto and S. Kitagawa, *Nat. Commun.*, 2011, **2**, 168.
15 G. Lu and J. T. Hupp, *J. Am. Chem. Soc.*, 2010, **132**, 7832–7833.
16 L. D. Bonifacio, B. V. Lotsch, D. P. Puzzo, F. Scotognella and G. A. Ozin, *Adv. Mater.*, 2009, **21**, 1641–1646.
17 S. John, *Phys. Rev. Lett.*, 1987, **58**, 2486–2489.
18 A. Arsenault, S. Fournier-Bidoz, B. Hatton, H. Miguez, N. Tetreault, E. Vekris, S. Wong, S. M. Yang, V. Kitaev and G. A. Ozin, *J. Mater. Chem.*, 2004, **14**, 781–794.
19 J. D. Joannopoulos, P. R. Villeneuve and S. Fan, *Nature*, 1997, **386**, 143–149.
20 H. Lee, *J. Appl. Phys.*, 2003, **93**, 819.
21 M. Bardosova, *Appl. Phys. Lett.*, 2006, **89**, 093116.
22 J. McPhillips, A. Murphy, M. P. Jonsson, W. R. Hendren, R. Atkinson, F. Höök, A. V. Zayats and R. J. Pollard, *ACS Nano*, 2010, **4**, 2210–2216.
23 R. Stine, J. T. Robinson, P. E. Sheehan and C. R. Tamanaha, *Adv. Mater.*, 2010, **22**, 5297–5300.
24 Z. Wang, J. Zhang, J. Xie, Z. Wang, Y. Yin, J. Li, Y. Li, S. Liang, L. Zhang, L. Cui, H. Zhang and B. Yang, *J. Mater. Chem.*, 2012, **22**, 7887–7893.
25 S. I. Khartsev, *Appl. Phys. Lett.*, 2005, **87**, 122504.
26 M. C. Fuertes, F. J. López-Alcaraz, M. C. Marchi, H. E. Troiani, V. Luca, H. Míguez and G. J. A. A. Soler-Illia, *Adv. Funct. Mater.*, 2007, **17**, 1247–1254.
27 S. Y. Choi, M. Mamak, G. von Freymann, N. Chopra and G. A. Ozin, *Nano Lett.*, 2006, **6**, 2456–2461.
28 J. Kobler, B. V. Lotsch, G. A. Ozin and T. Bein, *ACS Nano*, 2009, **3**, 1669–1676.
29 D. Lee, M. F. Rubner and R. E. Cohen, *Nano Lett.*, 2006, **6**, 2305–2312.
30 S. Colodrero, M. Ocaña, A. R. González-Elipe and H. Míguez, *Langmuir*, 2008, **24**, 9135–9139.
31 G. Lu, O. K. Farha, L. E. Kreno, P. M. Schoenecker, K. S. Walton, R. P. Van Duyne and J. T. Hupp, *Adv. Mater.*, 2011, **23**, 4449–4452.
32 Y.-n. Wu, F. Li, W. Zhu, J. Cui, C.-a. Tao, C. Lin, P. M. Hannam and G. Li, *Angew. Chem., Int. Ed.*, 2011, **50**, 12518–12522.
33 K. S. Park, Z. Ni, A. P. Côté, J. Y. Choi, R. Huang, F. J. Uribe-Romo, H. K. Chae, M. O'Keeffe and O. M. Yaghi, *Proc. Natl. Acad. Sci. U. S. A.*, 2006, **103**, 10186–10191.
34 J. M. Szeifert, J. M. Feckl, D. Fattakhova-Rohlfing, Y. Liu, V. Kalousek, J. Rathousky and T. Bein, *J. Am. Chem. Soc.*, 2010, **132**, 12605–12611.
35 J. Cravillon, S. Münzer, S.-J. Lohmeier, A. Feldhoff, K. Huber and M. Wiebcke, *Chem. Mater.*, 2009, **21**, 1410–1412.
36 B. V. Lotsch, F. Scotognella, K. Moeller, T. Bein and G. A. Ozin, *Proc. SPIE*, 2010, **7713**, 7713V.
37 C. Scherb, R. Koehn and T. Bein, *J. Mater. Chem.*, 2010, **20**, 3046–3051.
38 A. Demessence, C. Boissiere, D. Grosso, P. Horcajada, C. Serre, G. Ferey, G. J. A. A. Soler-Illia and C. Sanchez, *J. Mater. Chem.*, 2010, **20**, 7676–7681.
39 M. D. Allendorf, R. J. T. Houk, L. Andruszkiewicz, A. A. Talin, J. Pikarsky, A. Choudhury, K. A. Gall and P. J. Hesketh, *J. Am. Chem. Soc.*, 2008, **130**, 14404–14405.
40 G. Zhu, Y. Li, H. Zhou, J. Liu and W. Yang, *Mater.Lett.*, 2008, **62**, 4357–4359.
41 X.-L. Liu, Y.-S. Li, G.-Q. Zhu, Y.-J. Ban, L.-Y. Xu and W.-S. Yang, *Angew. Chem., Int. Ed.*, 2011, **50**, 10636–10639.
42 D. Fairen-Jimenez, S. A. Moggach, M. T. Wharmby, P. A. Wright, S. Parsons and T. Düren, *J. Am. Chem. Soc.*, 2011, **133**, 8900–8902.
43 M. Kodaka, *J. Phys. Chem. B*, 2003, **108**, 1160–1164.
44 J. Cousin Saint Remi, T. Rémy, V. Van Hunskerken, S. van de Perre, T. Duerinck, M. Maes, D. De Vos, E. Gobechiya, C. E. A. Kirschhock, G. V. Baron and J. F. M. Denayer, *ChemSusChem*, 2011, **4**, 1074–1077.

